Controlling Impurity-Induced Disordering Via Mask Strain for High-Performance Vertical-Cavity Surface-Emitting Lasers

Patrick Su, Thomas O'Brien, Jr., Fu-Chen Hsiao, John M. Dallesasse

University of Illinois at Urbana-Champaign, Department of Electrical and Computer Engineering, Urbana, Illinois, 61801
Tel: 1-(217)-333-8416, Email: psu8@illinois.edu, jdallesa@illinois.edu

Keywords: Vertical-cavity surface-emitting lasers, impurity-induced disordering, VCSEL aperture control, single-fundamental-mode VCSELs

Impurity-induced disordering (IID) in vertical-cavity surface-emitting lasers (VCSELs) has been shown to provide enhanced performance, such as achieving single fundamental-mode operation with higher output powers when compared to conventional VCSELs. This work presents the performance of oxide-confined, λ ~ 850 nm, VCSELs fabricated with varying IID aperture sizes which are characterized for maximum single-fundamental-mode output power. The electrical and optical performance of these devices are shown in comparison to traditional oxide-confined VCSELs and the optimal IID aperture size is experimentally validated. Control of the lateral-to-vertical (L/V) IID aperture profile is then demonstrated through engineering the strain induced by the IID diffusion mask. This extensive control over the IID aperture enables improved, manufacturable, IID VCSEL designs.

INTRODUCTION

The vertical-cavity surface-emitting laser (VCSEL) has become one of the most important semiconductor lasers in the market owing to its small footprint, low power consumption, and comparatively low manufacturing cost. VCSELs already play a significant role in data center optical links, optical communication networks, laser printing, and position sensors (optical computer mice). With the growing interest in using VCSELs for applications such as light detection and ranging (LIDAR) and 3D imaging, there is an increasing demand for a scalable method to produce high-performance VCSELs.

Impurity induced disordering (IID) was first discovered by Laidig *et al.* during the diffusion of Zn into an AlAs-GaAs superlattice [1]. The significance of impurity-induced disordering is found in its ability to intermix discrete direct band-gap AlGaAs-GaAs superlattices into a uniform alloy composition of bulk $Al_xGa_{1-x}As$ [2,3]. Since its discovery, a tremendous amount of research has been directed towards exploring the different superlattices and applications through leveraging IID's unique effects [2-4]. This maskable and planar technology became an attractive technology for wafer-scale applications and has been shown to provide significant performance enhancement in various optoelectronic devices [6-11]. In particular, disordering has been utilized to improve the performance characteristics of high-performance VCSELs. Enhancements such as higher modulation speeds [7], lower energy-to-data ratios [8], and greater output powers [9] than traditional VCSELs have been reported and disordering has also been shown as a method of mode suppression in VCSELs through shallow [10] and deep [11] impurity diffusions. This work explores the modal behavior of varying IID aperture sizes that are smaller than the oxide-aperture in order to highlight the effects of IID on the optical and electrical performance characteristics of VCSELs. Furthermore, this work introduces a novel method of controlling the IID aperture profile through altering the strain induced by the diffusion mask that enables improved aperture designs in IID VCSELs.

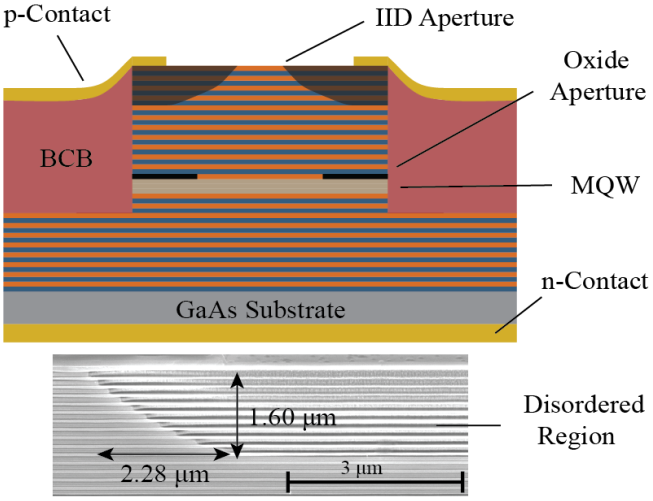

Fig 1. Cross-sectional schematic of an oxide-confined VCSEL with an IID aperture (top). A scanning electron microscope (SEM) image of the resulting disordered top DBR layer is shown (bottom).

DEVICE DESIGN AND FABRICATION

A cross-sectional schematic of the impurity-induced disordered VCSEL presented in this work is illustrated in

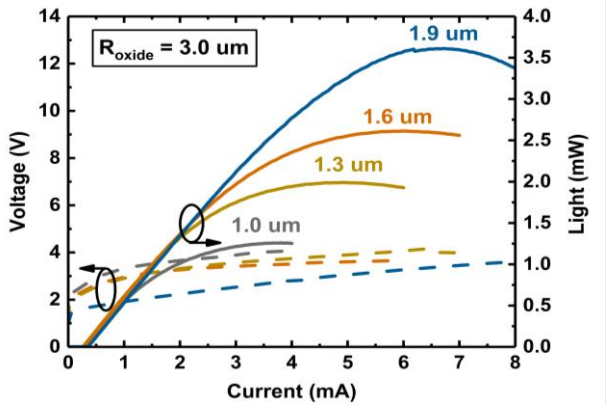

Fig 2. Light-current-voltage (LIV) characterizations of VCSELs with labeled varying IID aperture sizes and a fixed 3.0 μm oxide aperture [11].

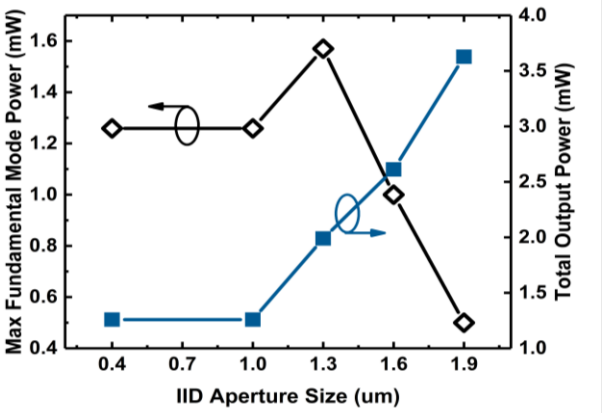

Fig 3. Varying IID aperture sizes with their corresponding maximum single-fundamental-mode output power [11].

Fig 1. The epitaxial structure consists of 37 *n*-type AlGaAs-based DBR pairs, 3 undoped GaAs quantum wells serving as the active region, and 20 *p*-type AlGaAs-based DBR pairs which are all grown on a GaAs substrate. A single high-aluminum content layer is grown directly above the active region and is formed into an oxide-aperture for electrical and optical confinement during fabrication [12,13]. It is noted that a GaAs cap layer is grown on top of the *p*-type DBR to improve current spreading. This cap layer is etched down to 100 nm to reduce phase-related mirror loss [14].

The devices were selectively disordered with Zn to form the IID apertures. In this work, the IID apertures were designed to be smaller than the oxide-confinement aperture. This makes the IID aperture the dominant aperture of the device due to a larger overlap with the optical modes as compared to the oxide aperture. The devices are masked with PECVD grown SiN_x - using a high-frequency (13.56 MHz) plasma source - to serve as a diffusion mask. The mask is lithographically patterned to open channels for disordering. The samples are placed in a quartz tube with a crystalline $ZnAs_2$ source and sealed-off under vacuum (< 5 x 10^{-6} Torr). Afterwards, the quartz ampoule is then loaded into a dry furnace to induce impurity disordering at 600°C for 80 minutes.

After the disordering process, the devices are then fabricated following a traditional oxide-confined VCSEL manufacturing process. Mesas are etched via Cl-based gases in an ICP-RIE dry etch system. Following the etch process, which is designed to expose the high-aluminum content layer for selective oxidation, the devices are loaded into a wet furnace at 405°C to form the oxide-confinement apertures. The devices are then planarized with benzocyclobutene (BCB) and then metallized with a top *p*-electrode layer (Ti/Pt/Au) via electron-beam evaporation. The GaAs substrate is then thinned down and planarized via chemical mechanical polishing (CMP). Subsequently, the bottom n-electrode layer (AuGe/Ni/Au) is deposited and then alloyed at 405°C to form an Ohmic backside contact.

DEVICE CHARACTERIZATION

Disordered and non-disordered VCSELs were characterized for electrical and optical performance comparisons. It was observed that introducing Zn during disordering in the top DBR also significantly reduced the series resistance of the device. The non-disordered VCSEL was measured to have a contact resistance of 146 Ω while the IID VCSEL was measured at only 56 Ω. This can be explained by the heavy additional p-doping that is introduced by diffusion of Zn into the top DBR layer, leading to a significant reduction in series contact resistance and the elimination of the low/high bandgap interfaces which can impede electron flow. Light-current-voltage (LIV) curves were then measured for varying IID aperture sizes as shown in Fig 2. All of the devices were designed to maintain an oxide aperture size of 3.0 μm in diameter while the IID aperture sizes were varied. Sweeping the IID aperture sizes provides an experimental analysis of how different IID aperture sizes affect the transverse optical modes and their maximum fundamental mode output power summarized in Fig 3. For a 1.0 um IID aperture device, the threshold current was measured to be 332 μA, which was the largest out of all the devices tested. This is expected since this device contains the largest IID region that has been shown to induce mirror loss and free-carrier absorption effects [9-12]. This device operated with a single fundamental mode throughout the entire current range. However, due to the largest amount of overlap between the IID region and the optical modes, the output power was also the lowest (0.5 mW) among the devices. As the IID aperture increased to 1.3 μm, the overlap between the disordered region and fundamental mode is reduced, which leads to a decrease in threshold current (271 μA) and an increase in fundamental mode power (0.8 mW). As the IID aperture increased further to 1.6 μm, the fundamental mode is no longer the only mode that does not have any overlap with the IID region and higher-order modes begin to lase as well.

This results in a decrease in fundamental mode output power even though the total output power increases. At an IID aperture size of 1.9 μm, the observed optical output is multi-modal with the lowest fundamental-mode output power. An analysis of these devices experimentally demonstrates an optimal IID aperture size of 1.3 μm. For this IID aperture size, the tradeoff between losses induced by the disordering region and its overlap with the higher-optical modes becomes optimized and exhibits the maximum fundamental-mode power (1.6 mW) of the devices studied. The LIV measurements taken also indicate that the thermal rollover current was larger for devices with smaller IID aperture sizes. This can be attributed to the observation that smaller IID aperture devices contain the largest impurity regions amongst the devices fabricated. These impurities contribute to increased free carrier absorption which heat the device.

CONTROL OF IID APERTURE SIZE

The benefits and properties induced by IID carry design tradeoffs dependent upon the varying lateral and vertical diffusion dimensions of the aperture. For instance, a deep impurity diffusion requires an increase in diffusion time. This consequently results in a wider lateral diffusion and can cause undesired overlap with the optical modes. It is apparent that the capability to form geometrically tailored diffusion fronts using this method is not feasible and limits the possibilities of IID aperture designs. This work introduces the ability to control the IID aperture profile through altering the strain induced by the diffusion mask. Utilizing a commercially available plasma-enhanced chemical vapor deposition (PECVD) tool that is equipped with a high-frequency (13.56 MHz) and low-frequency (680 KHz) plasma source, mixed compositions of high-frequency and low-frequency sourced SiN_x can be grown. Using a GaAs witness sample, it was measured that the high-frequency sourced SiN_x film induced a tensile strain of 347 MPa and the low-frequency sourced SiN_x film induced a compressive strain of -797 MPa. The significant difference in strain correspondingly results in distinctly geometrically different diffusion fronts as shown in Fig 4. In order to quantify the curvature of these diffusion fronts, the lateral-to-vertical (L/V) ratios of the diffusion front were measured using SEM images shown in Fig 4. Prior to imaging, the cleaved samples were stained with $K_3Fe(CN)_6$-KOH to enhance the contrast between the IID region and the non-disordered DBR [15].

Through periodically alternating the high-frequency and low-frequency source times, the strain of the diffusion mask can be engineered to any value in between the two limits. These masks will be designated as mixed-frequency films in this work. The two sources are periodically alternated until a total film thickness of 50 nm is reached with a time period of 20 seconds. The film stress of various mixed-frequency films was measured and fitted as shown in Fig 5. Mixed-frequency sourced diffusion masks that have a

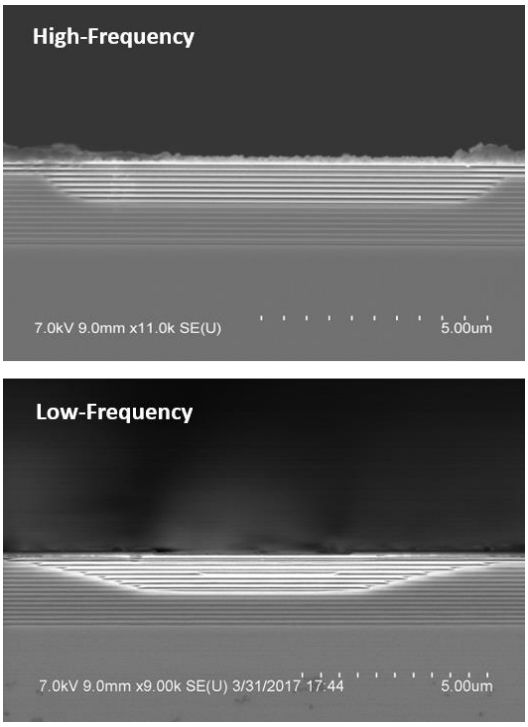

Fig 4. SEM images of stained IID apertures in DBR strained by a high-frequency sourced (top) and low-frequency sourced (bottom) PECVD grown SiN_x diffusion mask.

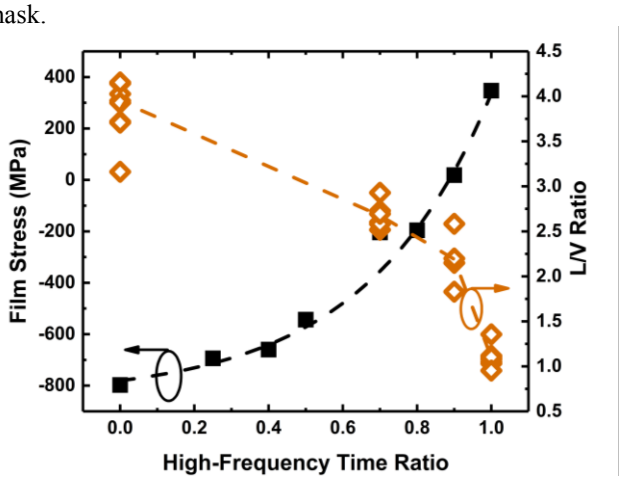

Fig 5. The change in IID aperture profile as a result of different strains induced by the diffusion mask.

high-frequency time ratio of 0.70 and 0.90 were then employed for disordering under the same conditions for the IID VCSELs fabricated in this work. As the diffusion mask moves towards a higher-frequency time ratio, the curvature of the IID aperture begins to approach the purely high-frequency case in a nearly-exponential trend. This suggests that the strain induced on the surface of the top DBR largely affects the geometrical structure and correspondingly the

diffusion front of the IID aperture. Furthermore, the exponential-like behavior in varying diffusion mask strain as a dependence of high-frequency time ratio is reflected in the L/V ratio of the resulting IID aperture. This method of controlling IID apertures enables the possibility of an array of IID aperture designs that can be used to optimize the performance enhancement effects of disordering in single-mode high-performance VCSELs.

CONCLUSION

The modal behavior of varying IID aperture sizes in oxide-confined VCSELs with their corresponding maximum single-mode output power is presented. The performance enhancement brought about by IID in VCSELs is experimentally demonstrated and an analysis of these effects are shown in this work. To leverage these effects, a manufacturable wafer-scale process of controlling the geometric structure of the IID aperture is presented. Through altering the strain induced by the diffusion mask, the geometric shape of the IID aperture can be extensively controlled. These results can be used to implement improved future IID aperture designs for enhanced high-power single-mode performance that are capable of being integrated into a large-scale manufacturing process.

ACKNOWLEDGEMENTS

This work is sponsored in part by E2CDA-NRI, a funded center of NRI, a Semiconductor Research Corporation (SRC) program sponsored by NERC and NIST under Grant No. NERC 2016-NE-2697-A and by the National Science Foundation under Grant No. ECCS 16-40196 and Grant No. NSF ACI 16-59293.

REFERENCES

[1] Laidig, W. D., et al. "Disorder of an AlAs-GaAs superlattice by impurity diffusion." *Applied Physics Letters* 38.10 (1981): 776-778.

[2] Holonyak, Nick. "Impurity-induced layer disordering of quantum-well heterostructures: Discovery and prospects." *IEEE Journal of Selected Topics in Quantum Electronics* 4.4 (1998): 584-594.

[3] Deppe, Dennis Glenn, and N. Holonyak Jr. "Atom diffusion and impurity-induced layer disordering in quantum well III-V semiconductor heterostructures." *Journal of applied physics* 64.12 (1988): R93-R113.

[4] Dallesasse, J. M., et al. "Impurity-induced layer disordering in In0. 5 (Al x Ga1− x) 0.5 P-InGaP quantum-well heterostructures: Visible-spectrum-buried heterostructure lasers." *Journal of Applied Physics* 66.2 (1989): 482-487.

[5] Thornton, Robert L., William J. Mosby, and Thomas L. Paoli. "Monolithic waveguide coupled cavity lasers and modulators fabricated by impurity induced disordering." *Journal of lightwave technology* 6.6 (1988): 786-792.

[6] Zou, W. X., et al. "Ultralow threshold strained InGaAs-GaAs quantum well lasers by impurity-induced disordering." *Electronics Letters* 27.14 (1991): 1241-1243.

[7] Shi, Jin-Wei., et al. "Minimization of damping in the electrooptic frequency response of high-speed Zn-diffusion single-mode vertical-cavity surface-emitting lasers." *IEEE Photonics Technology Letters* 19.24 (2007): 2057-2059.

[8] Shi, Jin-Wei., et al. "Oxide-relief and Zn-diffusion 850-nm vertical-cavity surface-emitting lasers with extremely low energy-to-data-rate ratios for 40 Gbit/s operations." *IEEE Journal of Selected Topics in Quantum Electronics* 19.2 (2013): 7900208-7900208.

[9] Shi, Jin-Wei., et al. "High-power and high-speed Zn-diffusion single fundamental-mode vertical-cavity surface-emitting lasers at 850-nm wavelength." *IEEE Photonics Technology Letters* 20.13 (2008): 1121-1123.

[10] Chen, C. C., et al. "Stable single-mode operation of an 850-nm VCSEL with a higher order mode absorber formed by shallow Zn diffusion." *IEEE Photonics Technology Letters* 13.4 (2001): 266-268.

[11] O'Brien, Thomas, et al. "Mode Behavior of VCSELs with Impurity-Induced Disordering." *IEEE Photonics Technology Letters* 29.14 (2017): 1179-1182.

[12] Huffaker, D. L., et al. "Native-oxide defined ring contact for low threshold vertical-cavity lasers." *Applied Physics Letters* 65.1 (1994): 97-99.

[13] Dallesasse, John M., and Dennis G. Deppe. "III–V oxidation: discoveries and applications in vertical-cavity surface-emitting lasers." *Proceedings of the IEEE* 101.10 (2013): 2234-2242.

[14] Kesler, Benjamin, et al. "Facilitating Single-Transverse-Mode Lasing in VCSELs via Patterned Dielectric Anti-Phase Filters." *IEEE Photonics Technology Letters* 28.14 (2016): 1497-1500.

[15] Buydens, L., et al. "Thickness variations during MOVPE growth on patterned substrates." *Journal of Electronic Materials* 19.4 (1990): 317-321.

ACRONYMS

DBR: Distributed Bragg Reflector
IID: Impurity Induced Disordering
L/V: Lateral-to-Vertical
LIV: Light-Current-Voltage
SEM: Scanning Electron Microscope
VCSEL: Vertical-Cavity Surface-Emitting Laser